RESEARCH ARTICLE

Enhanced Attachment and Collagen Type I Deposition of MC3T3-E1 Cells via Electrohydrodynamic Printed Sub-Microscale Fibrous Architectures

Shugang Hu[1,†], Zijie Meng[2,3,†], Junpeng Zhou[1], Yongwei Li[1], Yanwen Su[2,3], Qi Lei[2,3], Mao Mao[2,3], Xiaoli Qu[2,3], Jiankang He[2,3]*, Wei Wang[1]*

[1]Department of Bone and Joint Surgery, the Second Affiliated Hospital of Xian Jiaotong University, Xian Shaanxi, 710004, People's Republic of China
[2]State key laboratory for manufacturing systems engineering, Xi'an Jiaotong University, Xi'an, Shaanxi 710049, People's Republic of China
[3]NMPA Key Lab for Research and Evaluation of Additive Manufacturing Medical Devices, Xi'an Jiaotong University, Xi'an, 710049, China
†*These authors contributed equally to this work*

Abstract: Micro/sub-microscale fibrillar architectures of extracellular matrix play important roles in regulating cellular behaviors such as attachment, migration, and differentiation. However, the interactions between cells and organized micro/sub-microscale fibers have not been fully clarified yet. Here, the responses of MC3T3-E1 cells to electrohydrodynamic (EHD) printed scaffolds with microscale and/or sub-microscale fibrillar architectures were investigated to demonstrate their potential for bone tissue regeneration. Fibrillar scaffolds were EHD-fabricated with microscale (20.51 ± 1.70 μm) and/or sub-microscale (0.58 ± 0.51 μm) fibers in a controlled manner. The *in vitro* results showed that cells exhibited a 1.25-fold increase in initial attached cell number and 1.17-fold increase in vinculin expression on scaffolds with micro/sub-microscale fibers than that on scaffolds with pure microscale fibers. After 14 days of culture, the cells expressed 1.23 folds increase in collagen type I (COL-I) deposition compared with that on scaffolds with pure microscale fibers. These findings indicated that the EHD printed sub-microscale fibrous architectures can facilitate attachment and COL I secretion of MC3T3-E1 cells, which may provide a new insight to the design and fabrication of fibrous scaffolds for bone tissue engineering.

Keywords: Electrohydrodynamic printing; Micro/sub-microscale fibrous architectures; MC3T3-E1; Cell-scaffold interaction; Bone tissue engineering

*Correspondence to: Wei Wang, Department of Bone and Joint Surgery, the Second Affiliated Hospital of Xian Jiaotong, University, Xian Shaanxi, 710004, People's Republic of China; dr.wangwei@xjtu.edu.cn; Jiankang He, State key laboratory for manufacturing systems engineering, Xi'an Jiaotong University, Xi'an, Shaanxi 710049, People's Republic of China; jiankanghe@mail.xjtu.edu.cn

Received: December 6, 2021; **Accepted:** January 10, 2022; **Published Online:** February 11, 2022

Citation: Hu S, Meng Z, Zhou J, et al., 2022, Enhanced Attachment and Collagen Type I Deposition of Mc3t3-E1 Cells via Electrohydrodynamic Printed Sub-Microscale Fibrous Architectures. *Int J Bioprint,* 8(2):514. http://doi.org/10.18063/ijb.v8i2.514

1. Introduction

The extracellular matrix (ECM) of native bone exhibits filamentous nature, which consists of highly organized micro/nanoscale collagen fibers with hydroxyapatite and serves as crucial biophysical cues in regulating cellular behaviors for bone homeostasis[1-3]. Mimicking such fibrillar architectures in artificial implants is of great importance to restoring the biological functions of damaged bone tissues *in vitro*[4]. In this aspect, electrospinning technique has been widely utilized as a promising approach for the construction of bone tissue engineering scaffolds due to its unique capability in fabricating ECM-mimetic ultrafine fibers[5-7]. For example, Yao *et al*.[8] developed polycaprolactone (PCL) and polylactic acid composite fibrous scaffolds with

the fiber diameter ranging from 250 nm to 1 μm using electrospinning, which were found to facilitate attachment and osteogenic differentiation of human mesenchymal stem cells (hMSCs) *in vitro*. Ren *et al*.[9] fabricated electrospinning nanofibers membranes with different ratios of PCL/gelatin for guided bone regeneration. They found the fibrous membranes prompted calcium deposition of MC3T3-E1 cells both in growth media and osteogenic media. Nevertheless, the random deposition of the micro/sub-microscale fibers increases the complexity of the fibrous structures, which makes it difficult to decouple and decipher the interactions between the cells and the ECM-mimetic fibers[10-12].

Electrohydrodynamic (EHD) printing is a newly emerging method for fabricating fibrous scaffolds with ultrafine fibers and user-defined organizations[13]. Due to its capability of depositing every single fiber in a highly controlled manner, there has been an increasing interest in the investigation of cell-scaffold interactions using EHD printing[14-16]. For example, Brennan *et al*.[17] EHD-printed PCL microscale fibrous scaffolds with a fiber diameter of 4.01 μm and a fiber space ranging from 100 μm to 300 μm, and they found the scaffolds with the fiber space of 100 μm enhanced collagen and mineral deposition of hMSCs. Eichholz *et al*.[18] proposed microscale fibrous scaffolds (fiber diameter of 10.4 μm) with four types of fiber orientation angles (90°, 45°, 10°, and random) using EHD printing, which were further used to culture human skeletal stem cells (hSSCs). Their results indicated that scaffolds with orthogonal architectures enhanced osteogenesis of hSSCs via prompting yes-associated protein nuclear translocation. Xie *et al*.[19] investigated the effect of fiber diameter (3 – 22 μm) on the spreading behaviors of bone marrow stem cells (BMSCs) and human umbilical vein endothelial cells. They found that the BMSCs (with a size of 200 μm) preferred to adhere and bridge between thick fibers, while HUVECs (with a size of 100 μm) can only adhere to the microfibers and form a circle to gradually fill the pore space. However, the existing EHD-printed fibers are usually in microscale, and few studies have been conducted to investigate the response of cells on EHD-printed sub-microscale ECM-mimetic fibers.

We previously developed a solution-based EHD printing method for the fabrication of sub-microscale fibrous architectures[20]. The effect of sub-microscale fibers (about 0.5 μm) on rat myocardial cells was preliminarily investigated, with the results indicating that sub-microscale fibers could enhance cellular adhesion and orientation, whereas the effect of EHD-printed sub-microscale fibrillar architectures on bone cells' adhesion patterns, spreading morphologies, growth, migration, and osteogenic differentiation was not clear. Furthermore, solution-based EHD printing also provides an unprecedented opportunity to incorporate functional nanomaterials into the organized fibrous architectures for enhanced bioactivity[21,22]. Especially for osteogenic differentiation, nano hydroxyapatite (nHA) exhibits a strong componential similarity to native bones, which has been proven to be good osteoconductive and osteoinductive material[23,24]. Many existing studies have demonstrated that fibrous architectures with nHA can facilitate osteogenic differentiation[25,26]. For example, Li *et al*.[27] fabricated nHA/methacrylate gelatin/poly (l-lactic acid) electrospinning membranes with nHA concentration of 1% (nHA/solvent, w/v), which showed superior osteoinductivity compared to the membranes without nHA. However, few studies have realized organized sub-microscale fibrous architectures with nHA. In this study, we investigated the effect of the scaffolds with microscale and/or sub-microscale fibers on behaviors of MC3T3-E1 *in vitro*. The cellular attachment and spreading patterns were investigated by staining with vinculin and F-action. The osteogenic differentiation of MC3T3-E1 on scaffolds with microscale and/or sub-microscale fibers, and sub-microscale fibers with nHA was evaluated by detecting collagen type I (COL-I) deposition and alkaline phosphatase (ALP) after 14 days of culture.

2. Materials and methods

2.1. Materials

Medical-grade PCL was bought from Jinan Daigang Biomaterial Co., Ltd (Mw = 80,000 g/mol, China). Polyethylene oxide (PEO) was bought from Aladdin Co. Ltd (Mw = 300,000 g/mol, Italy). nHA was bought from Aladdin Reagent Co., LTD (China). For solution-based EHD printing of the sub-microscale fibrous architectures, PCL-PEO or PCL-PEO-nHA were dissolved or dispersed in acetic acid solution, and the content of which was set as 5% (w/v) for PCL, 6% (w/v) for PEO, and 0.5% (w/v) for nHA, respectively.

2.2. Design and EHD printing of fibrous scaffolds with micro/sub-microfibers

Three types of scaffolds with different structural and compositional organizations were designed and fabricated using EHD printing techniques (**Figure 1A-C**). The microscale fibrous scaffold (M) was designed with a fiber spacing of 300 μm, a cross angle at 90°, and a fiber offset of 150 μm (**Figure 1D**). The micro/sub-microscale fibrous scaffold (MS) was designed based on the M scaffolds, which contained sub-microscale fibers with a spacing of 100 μm. For fabrication, a total of five layers' microscale fibers and five layers' sub-microscale fibers were alternately stacked in a layer-by-layer manner (**Figure 1E**). The sub-microscale fibrous scaffold with nHA (MSN) shares the same structural organizations

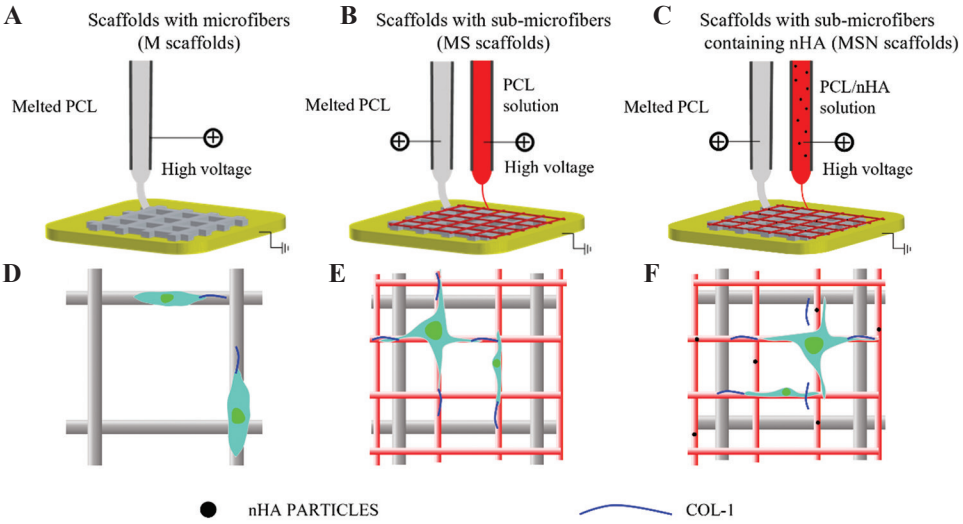

Figure 1. Schematic diagram for the fabrication and cellular responses on the fibrous scaffolds with different structural and componential organizations. Electrohydrodynamic printing of M scaffolds with microfibers (A), MS scaffolds with microscale and sub-microscale fibers (B), and MSN scaffolds with microscale and sub-microscale fibers containing nano hydroxyapatite (C). Illustration of cell morphology and COL-I secretion pattern on M (D), MS (E), and MSN (F) scaffolds are shown.

with MS scaffolds and contains 0.5% nHA in the sub-microscale fibers (**Figure 1F**).

To fabricate PCL microfibers, PCL raw materials were melted at 80°C in a glass syringe, and an ITO glass was used as the collecting substrate. The nozzle gauge was 20G and the nozzle to collector distance was set as 5 mm. The voltage, feeding rate, and stage moving speed were fixed at 4.6 kV, 30 μl/h, and 35 mm/s, respectively. To fabricate the sub-microscale fibrous architectures, solution-based EHD printing process was employed[20]. The nozzle gauge was 34G and the nozzle to collector distance was set as 2 mm. The voltage, feeding rate, and stage moving speed were fixed at 0.8 kV, 50 nl/min, and 150 mm/s, respectively.

After fabrication, the morphology of the micro/sub-microscale fibrous scaffolds was characterized by emission scanning electronic microscopy (SEM, SU8010, Hitachi, Japan). The fiber diameter was further measured by ImageJ software from the SEM images. The existence of nHA in the sub-microfibers was characterized by an energy-dispersive X-ray spectrometry with an elemental analyzer (EDS, Vario EL cube, ELEMENT, Germany).

2.3. MC3T3-E1 cell culture on fibrous scaffolds with micro/sub-microfibers

To investigate the responses of cells on the fibrous scaffolds with different fiber diameters for potential bone regeneration applications, the mouse pre-osteoblast cell line, MC3T3-E1 (Cell Bank of the Chinese Academy of Sciences, Shanghai, China) was used. The cells were cultured in an alpha-minimum essential media (α-MEM, Biological Industries, Israel) supplemented with 10% fetal bovine serum (Biological Industries, Israel) and 1% penicillin/streptomycin (Biological Industries, Israel). Before cell seeding, the scaffolds were punched to have a round shape with a diameter of 15 mm and placed into a 24-well culture plate, which were then fixed by glass rings and sterilized using 75% alcohol aqueous solution. Cells were then seeded at a density of 5×10^4 cells per scaffold and cultured in a humidified incubator with 5% CO_2 at 37°C.

2.4. Initial adhesion behaviors of MC3T3-E1 on scaffolds with micro/sub-microfibers

To investigate the effect of scaffolds with micro/sub-microscale fibers on the initial adhesion numbers of MC3T3-E1 cells, a live/dead viability/cytotoxicity kit (Invitrogen, USA) was used for staining the attached cells after 4 h of culture. Cell-scaffold constructs were washed with phosphate-buffered saline (PBS) for 3 times and then incubated in staining solutions for 30 min. An inverted laser confocal microscope (A1, Nikon, Japan) was employed to measure the living cell numbers attached on the scaffolds, which were further standardized by the image area to calculate the initial adhesion density of the fibrous scaffolds.

To further evaluate the MC3T3-E1 adhesion patterns on micro/sub-microscale fibers, the cell-scaffold constructs were fixed with 4% formaldehyde and then triple-stained with vinculin, F-actin, and nuclear after 24 h of culture. After permeabilized by 0.3% Triton X-100 and blocked by 5% bovine serum albumin (BSA), the cell-scaffold constructs were incubated with primary antibodies (Recombinant Anti-Vinculin antibody, ab129002, Abcam, USA) overnight at 4°C. Then the

constructs were further incubated with Alexa Fluor 488-conjugated goat anti-rabbit IgG H&L (ab150077, Abcam, USA) secondary antibodies for 60 min. Finally, F-actin was stained with Alexa Fluor 594 phalloidin for 30 min and cell nuclear was stained with DAPI for 5 min. Cells were visualized by laser confocal fluorescence microscope. For each sample, the fluorescence images were captured with a total thickness of 60 μm and a z-step of 5 μm. The fluorescence intensity was then measured on the maximum projection stacks of the vinculin channel by Image J software[7].

2.5. MC3T3-E1 morphology, migration on scaffolds with micro/sub-microfibers

Cell morphology and migration were visualized by staining cellular F-actin and nucleus with phalloidin and DAPI after 4 h, 24 h, 4 days, and 7 days of culture using previously described methods. The fluorescence images of the cells on the scaffolds were captured with a total thickness of 25 μm and a z-step of 5 μm. Cell projection area and cell aspect ratio were defined as critical parameters for the evaluation of cellular morphology. Cell projection area was measured by manually drawing the outlines of F-actin on the maximum projection stacks of the F-actin channel and cell aspect ratio was obtained by calculating the ratio of the major to minor axis of the cells[18]. The cell-scaffold constructs were gradually dehydrated by ethyl alcohol and the cellular morphology was further observed with SEM[28].

2.6. Osteogenic differentiation of MC3T3-E1 on scaffolds with micro/sub-microfibers

The osteogenic differentiation of MC3T3-E1 cells on scaffolds with micro/sub-microscale fibers was analyzed by COL-I immunofluorescence staining, ALP staining, and ALP activity. Cells were seeded at a density of 2×10^5 cells per scaffold and cultured for 14 days. Osteoblastic phenotypic maturation of MC3T3-E1 cells was analyzed by immunofluorescence staining of COL-I. After being fixed with 4% formaldehyde, followed by permeabilized by 0.3% Triton X-100 and blocked by 5% BSA, the cell-scaffold constructs were incubated with primary antibodies (COL1A1 (E8F4L) XP Rabbit mAb, 72026, and Cell Signaling Technology, USA) overnight at 4°C. Next, the samples were incubated with Alexa Fluor 555-conjugated anti-rabbit IgG H&L (4413, Cell Signaling Technology, USA) secondary antibodies for 60 min. Cell nucleus was stained with DAPI for 5 min. The COL-I was viewed using the confocal laser scanning microscope, and the amount of the deposited COL-I was quantified using Image J software[29].

ALP was stained using BCIP/NBT ALP color development kit (Beyotime, China) according to the manufacturer's protocol. Briefly, the cell-scaffold constructs were washed with PBS for 3 times and fixed with 4% formaldehyde for 30 min. Then the constructs were incubated in BCIP/NBT solutions for 60 min. For measuring the ALP activity, the cell-scaffold constructs were washed with cold PBS (4°C) for 3 times and lysed in RIPA lysis buffer (strong, without inhibitors, Beyotime, China). After centrifugation at 11,000 relative centrifugal force (rcf) for 20 min, the supernatant was collected and the amount of converted p-nitrophenol was measured using the p-nitrophenyl phosphate (PNPP) assay. The total amount of protein was evaluated by a bicinchoninic acid protein assay kit (BCA, Beyotime, China) with BSA serving as standard protein samples. The ALP activities of MC3T3-E1 cells were finally quantified by standardization of the amount of converted p-nitrophenol with the corresponding reaction time and the total amount of proteins.

2.7. Statistical analysis

The quantified and semi-quantified data were presented as mean ± standard deviation. Statistical analysis was performed using one-way statistical analysis of variance (ANOVA) followed by Tukey *post hoc* test with GraphPad software. $P < 0.05$ (*) was considered as statistical difference.

3. Results and discussion

3.1. Characterization of micro/sub-microscale fibrous scaffolds

Figure 2 shows the SEM images of EHD-printed M, MS, and MSN scaffolds with orthogonal microfibers (**Figure 2A**), microscale and sub-microscale fibers (**Figure 2B**) as well as microscale and sub-microscale fibers containing nHA (**Figure 2C**), respectively. It can be observed that the microfibers can be regularly deposited according to the designed trajectory with a smooth surface morphology in each type of scaffold. In contrast, the deposited sub-microscale fibers exhibited a less regular organization, as the ultrafine fibers are very tiny and extremely susceptible to electrostatic repulsion and attraction force derived from previously deposited fibers. Besides, the sub-microscale fibers with nHA possessed a larger diameter compared to PCL-PEO sub-microscale fibers (**Figure 2C**). The diameters of EHD-printed microfibers, sub-microscale fibers, and sub-microscale fibers with nHA were measured as 20.51 ± 1.70 μm, 0.58 ± 0.13 μm, and 0.62 ± 0.11 μm, respectively (**Figure 2D**). The size of the sub-microscale fibers with or without nHA showed no statistical differences and was close to the scale of collagen fibrils (<500 nm)[30]. The presence of nHA in sub-microscale fibers was further verified using EDS profiles. Calcium and phosphorus elements were detected in sub-microscale fibers with nHA

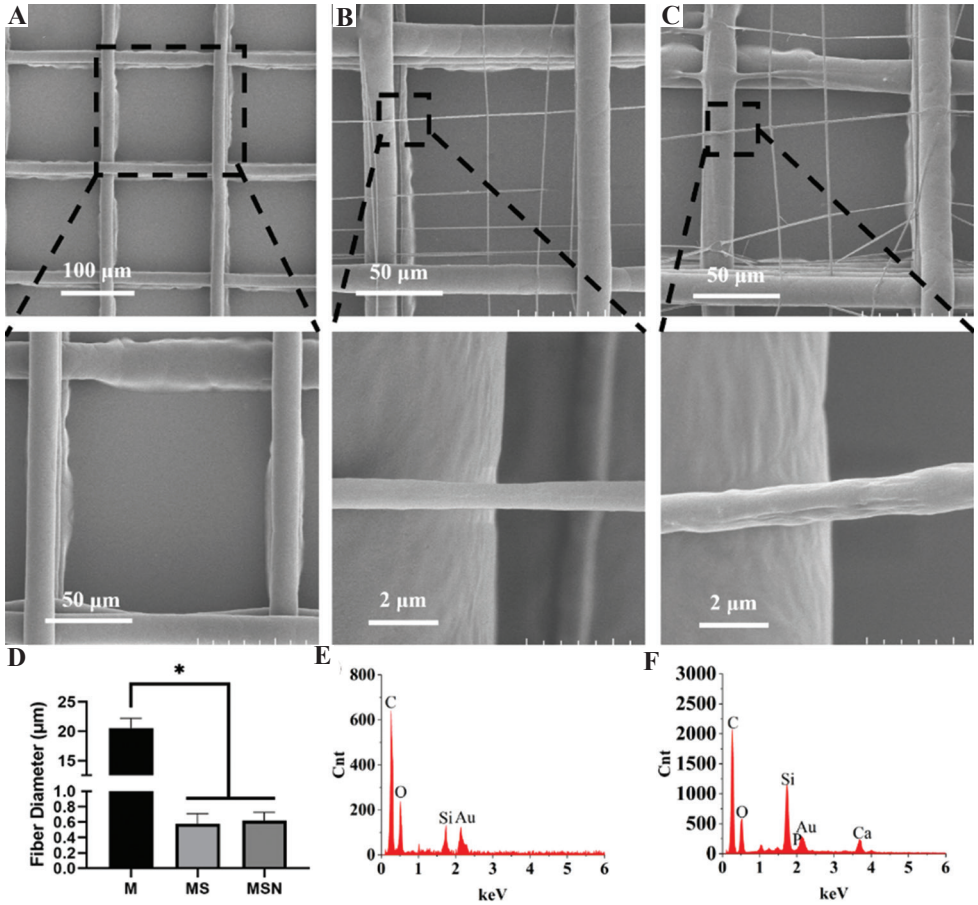

Figure 2. Characterization of the structure and component of scaffolds with microscale and sub-microscale fibers. (A–C) Scanning electronic microscopy images of M, MS, and MSN scaffolds, respectively. (D) Diameters of the electrohydrodynamic-printed microscale and sub-microscale fibers. (E) EDS spectrum of pure polycaprolactone sub-microscale fiber. (F) Sub-microscale fiber with nano hydroxyapatite. *$P < 0.05$.

(**Figure 2F**), which were absent in microscale fibrous PCL architectures (**Figure 2E**).

We also tried to print sub-microscale PCL fibers with a higher nHA concentration (e.g., 1%, 2%, and 4%). As shown in **Figure S1A**, nHA nanoparticles were found to sparely decorate in the sub-micron PCL fibers when the nHA concentration was 0.5%. The resultant fibers were continuous and showed smooth surface. By contrast, obvious nHA aggregates appeared in the fibers with the increase of the nHA concentration to 1%, 2%, and 4% (**Figure S1B-D**). These uneven distribution of nHA within PCL solutions resulted in non-uniform Coulomb force between the nHA aggregates in the polymer jet, which thus affected the stability of EHD printing. Meanwhile, the printed fibers exhibited a ribbon-like morphology with a larger feature size of 1.10 ± 0.31, 1.33 ± 0.45, and 2.16 ± 0.80 μm as the nHA concentration increased from 1% to 4%, respectively.

More importantly, we found that a higher concentration of nHA over 0.5% inside the PCL solution disturbed the stability of EHD printing process, causing fracture of ultrafine fibers at the intersection site of sub-microscale fibers and microfibers, as shown in the SEM images of **Figure S2**. This will further cause the instability and floating of tiny fibers during cell culture period. Therefore, the cell culture experiment was only conducted for the EHD-printed architectures with a nHA concentration of 0.5%.

3.2. MC3T3-E1 initial adhesion behaviors on scaffolds with micro/sub-microfibers

Figure 3A-C present the live/dead staining of the cells attached on the porous scaffolds after 4 h of culture. The attached MT3T3-E1 cell showed high viability on each type of scaffold, indicating good biocompatibility of the fibrous architectures. The cells were found to uniformly distribute on M scaffolds with only a few cells decorated on the microfibers (**Figure 3A**). By contrast, the cells can adhere on both microscale and sub-microscale fibers of MS and MSN scaffolds, resulting in a relatively high cellular density (**Figure 3B and C**). The numbers of

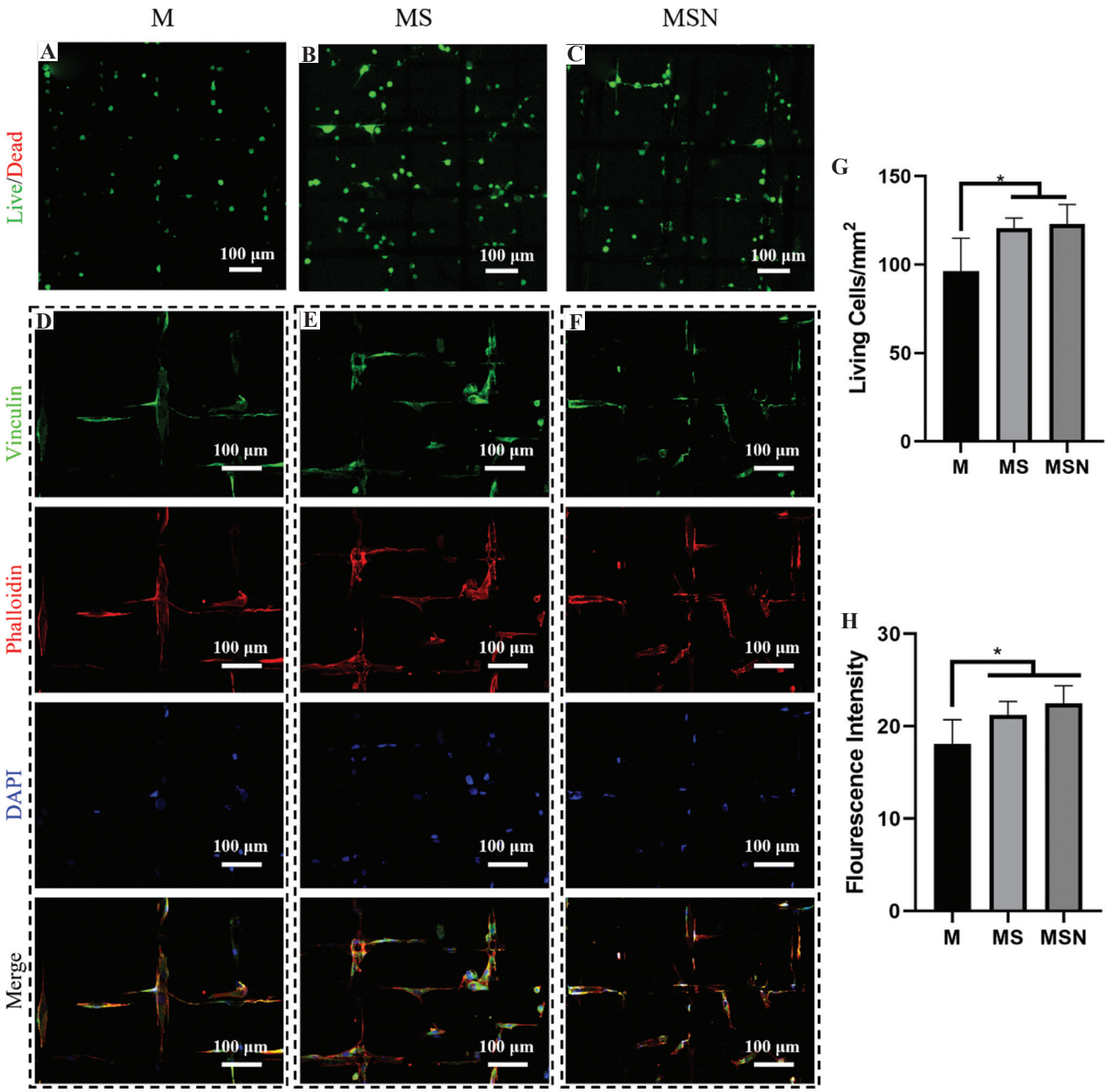

Figure 3. Effect of scaffolds with micro/sub-microscale fibers on MC3T3-E1 initial adhesion behaviors. (A–C) Live/dead staining of cells on M, MS, and MSN scaffolds, respectively. (D–F) Vinculin immunofluorescence staining of cells on M, MS, and MSN scaffolds, respectively. (G) Average living cell numbers on M, MS, and MSN scaffolds. (H) Semi-quantified results of vinculin fluorescence intensity. *$P < 0.05$.

attached living cells were then counted using ImageJ software and standardized by image area. As shown in **Figure 3G**, M, MS, and MSN scaffolds possessed a cellular density of 96.31 ± 18.58, 120.70 ± 5.62, and 122.80 ± 11.15 cells/mm^2, respectively. The cell numbers were almost the same on MS and MSN scaffolds, which were 1.25- and 1.28-fold higher than that on M scaffolds. This phenomenon is in good agreement with previous literature, which reported a higher number of attached cells on scaffolds with sub-microscale fibers than that on scaffolds with pure microfibers[31,32].

Focal adhesions are believed to be positively associated with cell attachment, morphology, migration, and mechanosensory[33,34]. In our study, vinculin, an intracellular component of focal adhesion that mediates the interaction between integrins and actin[35] was detected to investigate the adhesion patterns of cells on scaffolds with micro/sub-microscale fibers. As showed in **Figure 3D-F**, vinculin,

F-actin and nuclei of the MT3T3-E1 cells were represented with green, red, and blue fluorescence, respectively. The confluence of vinculin and F-actin confirmed the cytoplasm localization of vinculin, which were partially adhered on the microfibers (**Figure 3D**) and completely wrap the sub-microscale fibers (**Figure 3E and F**). This finding demonstrated that the cell exhibited a firm interaction with sub-microscale fibers. Semi-quantification of vinculin expression through measuring fluorescence intensity was further shown in **Figure 3H**. The fluorescence intensity of vinculin on MS and MSN scaffolds was 21.22 ± 0.90 and 22.47 ± 1.77, which were 1.17- and 1.24-fold higher than that on M scaffolds. However, no significant difference was observed between the mean fluorescence intensity on MS and MSN scaffolds. The improved cellular adhesion behaviors on the sub-microscale fibrous architectures can be attributed to the morphology of the ultrafine fibers, which provide unique contact cues for cell membrane to warp[31].

3.3. Cell spreading morphology on scaffolds with micro/sub-microfibers

We further analyzed the cell morphology on porous scaffolds with different fiber sizes and organizations.

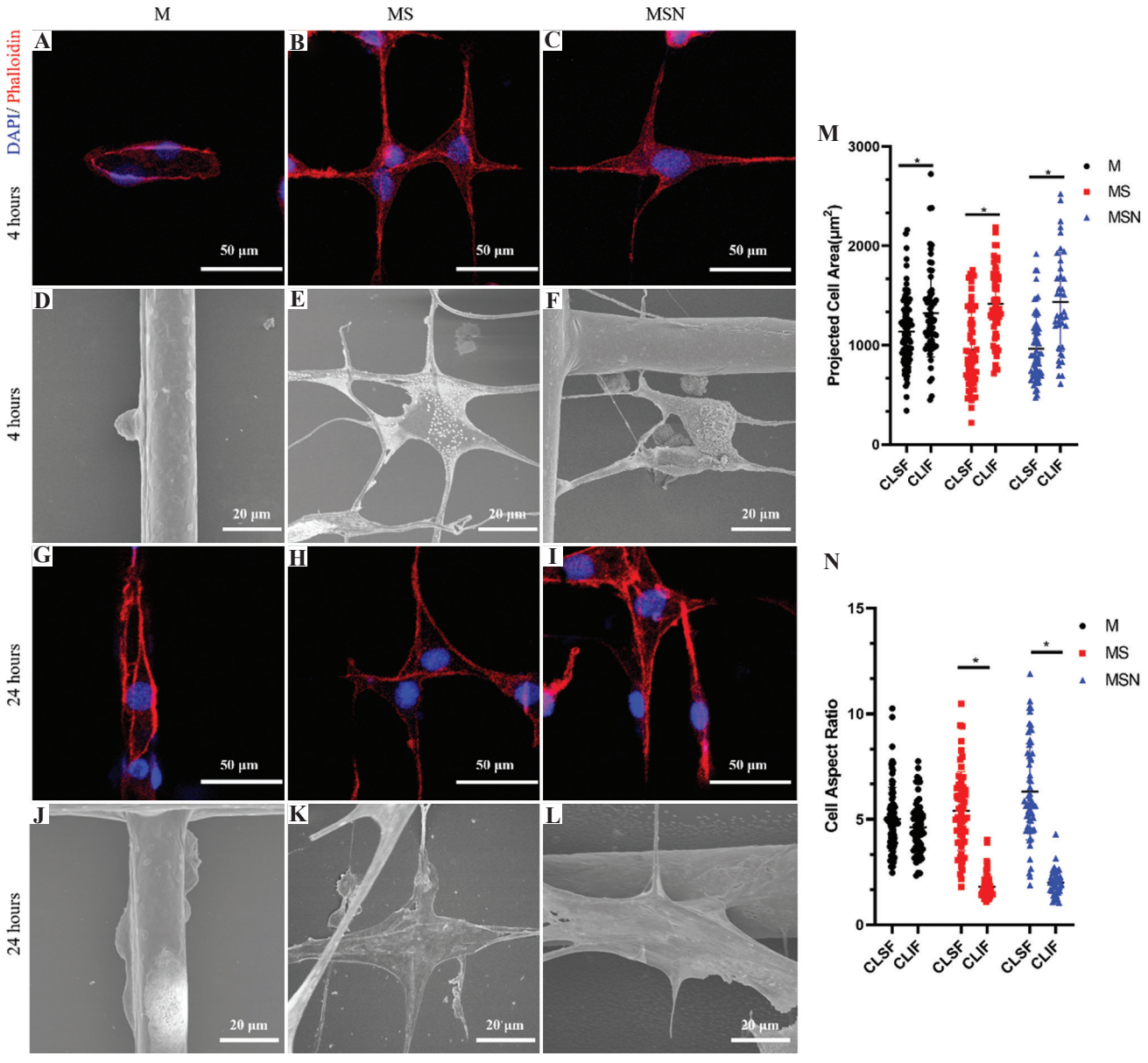

Figure 4. Cell spreading morphology on scaffolds with micro/sub-microscale fibers. F-actin staining of cells on M, MS, and MSN scaffolds after 4- (A–C) and 24- (G–I) hour of culture. SEM images of cells on M, MS, and MSN scaffolds after 4- (D–F) and 24- (J–L) hour of culture. Quantitative cell projection area (M) and aspect ratio (N) after 24 h of culture. CLSF, cells located at single fiber; CLIF, cells located at intersection of fibers. *$P < 0.05$.

Figure 4 shows fluorescent and SEM images of the cytoskeleton of the seeded MC3T3-E1 cells. After 4 h of culture, cells remained a round shape morphology on microfibers of M scaffolds (**Figure 4A and D**). By contrast, the cells were found to spread on sub-microscale fibers of MS (**Figure 4B and E**) and MSN scaffolds (**Figure 4C and F**). After cultured for 24 h, cells spread along both micro and sub-microfibers with an elongated morphology (**Figure 4G-L**). It is interesting to note that the cells exhibited different morphologies depending on fiber size and structural locations. At the intersection of sub-microfibers, cells were polygonal and showed a large cell projection area (**Figure 4M**). When the cells spread on a single sub-microfiber, they were fusiform with a high cell aspect ratio (**Figure 4N**). Similar phenomenon has also been observed when culturing mouse C2C12 cells on polystyrene nanofibers[36]. On the other hand, the cells exhibited oval shape on microfibers regardless of the location, which showed a relatively large projection area and small aspect ratio (**Figure 4M and N**).

3.4. MC3T3-E1 cells growth and migration on scaffolds with micro/sub-microfibers

Bone-related cells are recruited to the injured region during the tissue regeneration process[37], which requires the scaffolds to be well osteoconductive[38]. F-actin staining was used to track the distribution and migration of MC3T3-E1 cells on the scaffolds with micro/sub-microscale fibers (**Figure 5**). As shown in **Figure 5A**, MC3T3-E1 cells were found to spread on microfibers of the M scaffolds after 1 day of culture, which gradually proliferated and migrated along the microfibers on day 4 (**Figure 5D**). Some pores between the microfibers were found to be bridged and filled with cells on day 7 (**Figure 5G**). In contrast, cells on MS scaffolds can attach and spread on both microscale and sub-microscale fibers after cultured for 1 day (**Figure 5B**). With the guidance of sub-microscale fibers, the cells quickly migrated into the spacing between fibers on day 4 (**Figure 5E**) and finally formed interconnected cellular networks on day 7 (**Figure 5H**). Similar phenomena were also observed

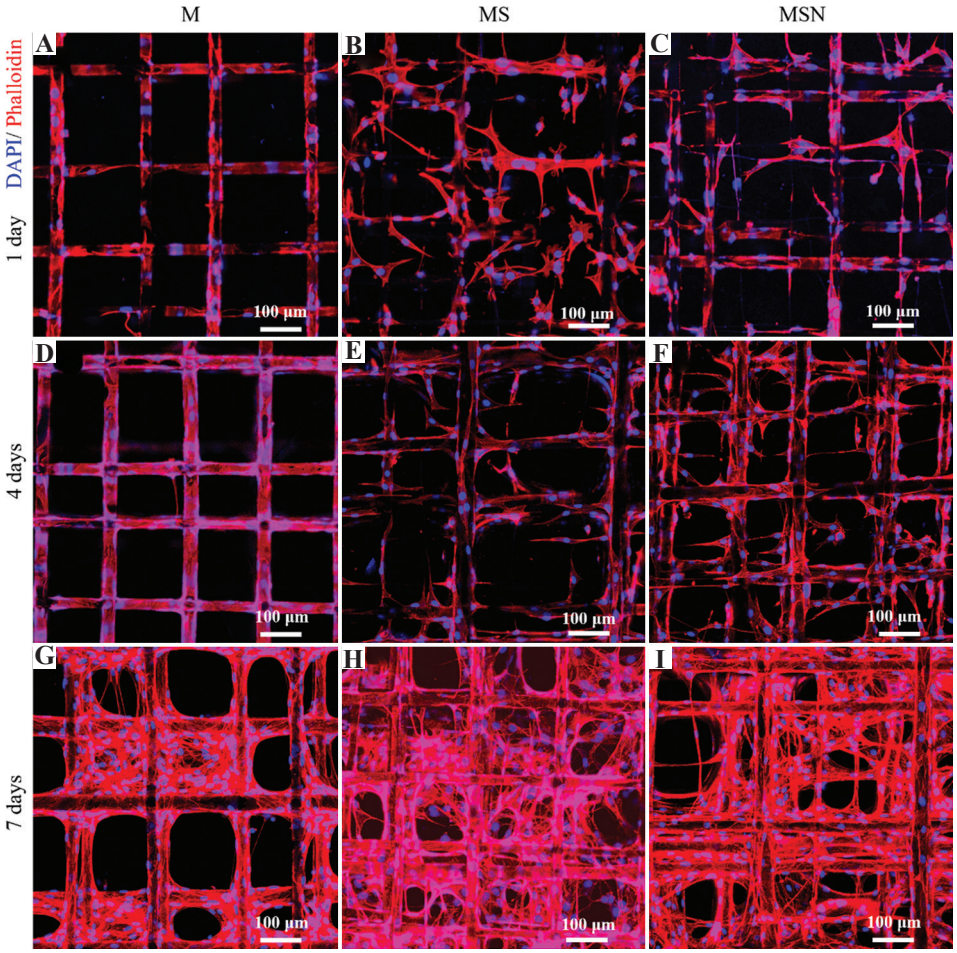

Figure 5. Effect of scaffolds with micro/sub-microscale fibers on MC3T3-E1 cells migration. Migration and distribution of cells on M, MS, and MSN scaffolds on day 1 (A–C), 4 (D–F), and 7 (G–I), respectively.

in MSN scaffolds (**Figure 5C, F and I**). These results evidenced that the scaffolds with sub-microscale fibers can facilitate the spreading and migration of cells to cover the whole scaffold, which resulted in a more uniform cellular distribution. In addition, these findings provide an innovative approach to designing tissue analogs with desirable cellular morphologies and distributions. For example, heterogeneous scaffolds with variable fiber size and controlled fibrous organizations can be fabricated for directing the cellular morphology, migration, and distribution to meet specific tissue demands.

3.5. Osteogenic differentiation of MC3T3-E1 on scaffolds with micro/sub-microfibers

As a major organic component of bone matrices, COL-1 is directly synthesized and secreted by bone cells during bone regeneration process[38]. In addition, ALP degrades phosphate-containing compounds to produce phosphate ions, which plays an essential role in the formation of hydroxyapatite crystals of bone matrices[39]. In this study, COL-I immunofluorescence staining, ALP staining, and ALP activity measurement were conducted on day 14 to evaluate the osteogenic differentiation of MC3T3-E1 cells. As shown in **Figure 6A-C**, COL-I was found around the MC3T3-E1 cells in all scaffolds. Obviously denser secretion of COL-I was observed on MS and MSN scaffolds, with the semi-quantified results showing 1.23- and 1.25-fold higher COL-I fluorescence intensity than that on M scaffolds (**Figure 6G**).

ALP staining of different scaffolds exhibited very similar trends (**Figure 6D-F**), which was further quantitatively analyzed in **Figure 6H**. It was found that the ALP activity increased to 8.68 ± 1.68 nmol/min/mg protein compared to that of M and MS scaffolds, which were 7.34 ± 1.34 and 6.89 ± 0.67 nmol/min/mg protein. However, the result showed no statistical difference. On the basis of these findings, the EHD-printed PCL scaffolds

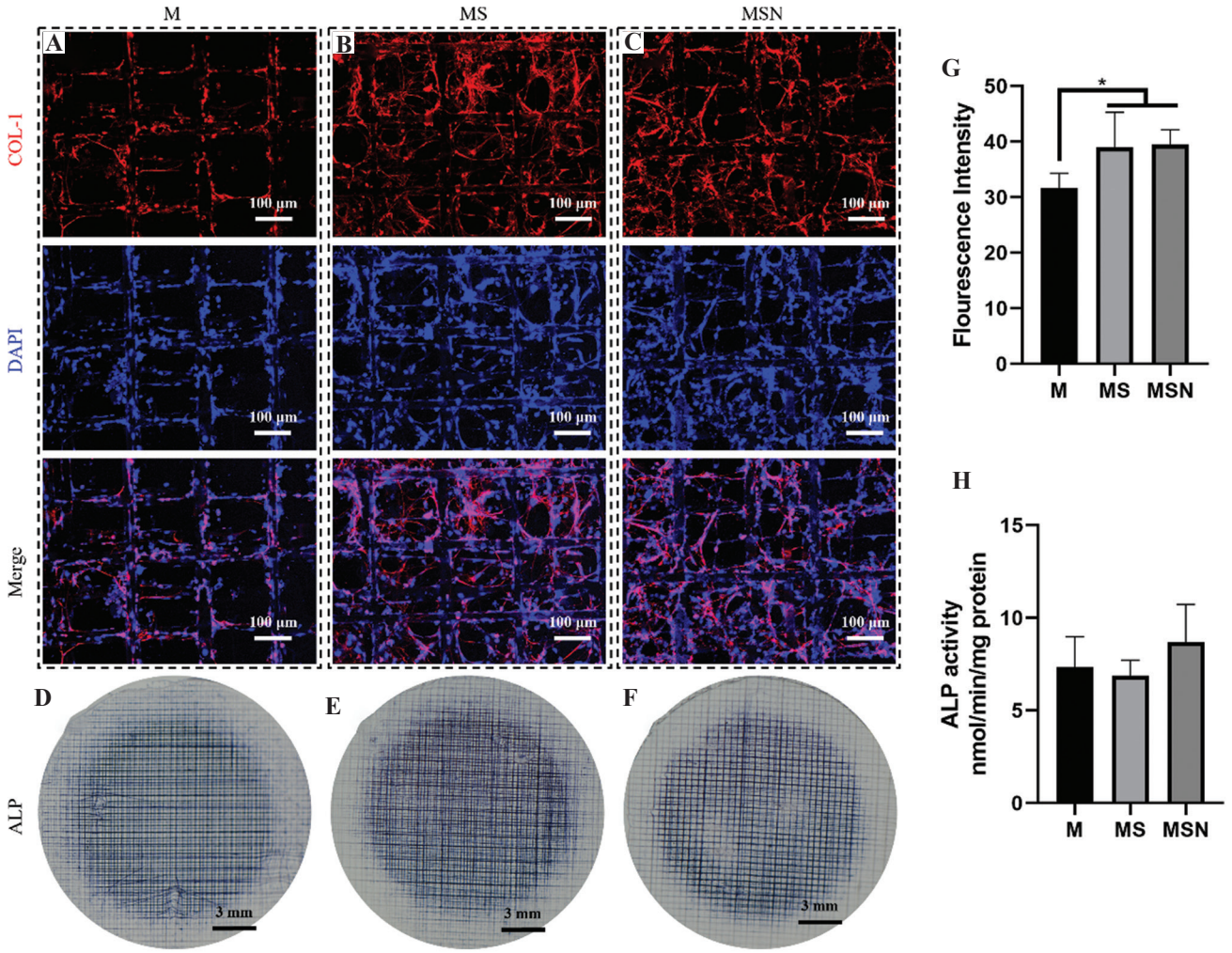

Figure 6. Effects of scaffolds with micro/sub-microscale fibers on MC3T3-E1 cells' osteogenic differentiation. (A–C) COL-I immunofluorescence staining of M, MS, and MSN scaffolds, respectively. (D–F) ALP staining of M, MS, and MSN scaffolds, respectively. Semi-quantified results of COL-1 fluorescence intensity (G) and normalized ALP activity (H) are shown. *$P < 0.05$.

with sub-microscale fibers can direct the osteogenic differentiation through prompting organic component deposition (COL-I), while the sub-microscale fibrillar architectures have little effect on ironic component formation.

A series of life activity of bone-related cells was involved during the regeneration of bone tissues. Namely, cells are recruited to the defect areas and then proliferate and differentiate to specific functional cell lines[40,41]. Here, we fabricated scaffolds with microscale and/or sub-microscale fibrillar architectures, and mouse pre-osteoblast cell line MC3T-E1 was used to demonstrate their potential for bone tissue regeneration. Cells initial adhesion behaviors on scaffolds were investigated since cellular migration is largely dependent on focal adhesion[34]. Our results showed that cells on scaffolds with sub-microscale fibers expressed more focal adhesion and can quickly spread and migrated into the spacing between fibers with the guidance of sub-microfibers. The differentiation of MC3T3-E1 cells were evaluated by ALP activity and COL-I expression, with the results showing that scaffolds with sub-microfibers prompted COL-I deposition while have little effect on ALP activities.

It should be noted that there are several limitations in this study. About 0.5% nHA was added to sub-microscale fibrous architectures successfully and we found that the ALP activity did increase to 8.68 ± 1.68 nmol/min/mg protein compared to that of micro/sub-microscale fibrous architecture without nHA (6.89 ± 0.67 nmol/min/mg protein). However, due to the small size of nHA (about 50 nm), most nHA particles were entrapped inside the sub-microscale PCL fibers (>500 nm), which might be the main reason for no significant statistical difference in the ALP results. One promising solution to improve bioactivity of the MS scaffolds in the future is to coat or self-assemble functional nanomaterials on the surface of micro/sub-microscale fibrous architectures. Furthermore, the effectiveness of the sub-microscale fibrous architectures to promote bone regeneration should be further evaluated *in vivo* for future clinical applications.

4. Conclusion

In the present study, we fabricated ECM-mimetic scaffolds with microscale and/or sub-microscale fibrillar architectures. The average diameter of microfibers and sub-microscale fibers is 20.51 ± 1.70 μm and 0.58 ± 0.51 μm, respectively. We found that the scaffolds with sub-microscale fibers could enhance MC3T3-E1 cell's initial attachment, regulate cell spreading morphology, facilitate cell migration, and prompt COL-I deposition *in vitro* compared to the scaffolds with pure microfibers. These results primarily demonstrated the potential capability of scaffolds with sub-microscale fibers for bone tissue engineering.

Acknowledgments

The authors sincerely thank Dr. Liying Liu at the Biomedical Experimental Center of Xi'an Jiaotong University Health Science Center for her assistance with cell culture and laser scanning confocal microscope experiments.

Funding

This work was financially supported by the National Natural Science Foundation of China (82072522, 52125501, and 31971272), the Integrated Traditional Chinese and Western Medicine Clinical Collaboration Innovation Project of Shaanxi Administration of Traditional Chinese Medicine (2020-ZXY-003), the Key Research Project of Shaanxi Province (2020GXLH-Y-001, 2020GXLH-Y-021, 2021GXLH-Z-028), Guangdong Basic and Applied Basic Research Foundation (2020B1515130002), The Youth Innovation Team of Shaanxi Universities and the Fundamental Research Funds for the Central Universities.

Conflict of interest

The authors declare no competing financial interest.

Author contributions

S.H., Z.M., Y.S., and X.Q. designed the experimental plan and conducted the experiments. S.H. wrote the manuscript with support from Z.M., J.H., and W.W. Detailed research results were collected and reviewed by J.Z., Y.L, Q.L, and M.M. J.H. and W.W. supervised the project and conceived the original idea.

References

1. Eliaz Nand Metoki N, 2017, Calcium Phosphate Bioceramics: A Review of Their History, Structure, Properties, Coating Technologies and Biomedical Applications. *Materials (Basel)*, 10:334.
https://doi.org/10.3390/ma10040334
2. Florencio-Silva R, Sasso G R, Sasso-Cerri E, *et al.*, 2015, Biology of Bone Tissue: Structure, Function, and Factors That Influence Bone Cells. *Biomed Res Int*, 2015:421746.
https://doi.org/10.1155/2015/421746
3. Lin X, Patil S, Gao Y G, *et al.*, 2020, The Bone Extracellular Matrix in Bone Formation and Regeneration. *Front Pharmacol*, 11:757.
https://doi.org/10.3389/fphar.2020.00757
4. Hogrebe NJ, Reinhardt JW, Gooch KJ, 2017, Biomaterial Microarchitecture: A Potent Regulator of Individual Cell Behavior and Multicellular Organization. *J Biomed MATER Res A*, 105:640–61.

https://doi.org/10.1002/jbm.a.35914

5. Xue J, Wu T, Dai Y, *et al.*, 2019, Electrospinning and Electrospun Nanofibers: Methods, Materials, and Applications. *Chem Rev*, 119:5298–415. https://doi.org/10.1021/acs.chemrev.8b00593
6. Nekounam H, Samadian H, Bonakdar S, *et al.*, 2021, Electro-Conductive Carbon Nanofibers Containing Ferrous Sulfate for Bone Tissue Engineering. *Life Sci*, 282:119602. https://doi.org/10.1016/j.lfs.2021.119602
7. Wu L, Gu Y, Liu L, *et al.*, 2020, Hierarchical Micro/Nanofibrous Membranes of Sustained Releasing VEGF for Periosteal Regeneration. *Biomaterials*, 227:119555. https://doi.org/10.1016/j.biomaterials.2019.119555
8. Yao Q, Cosme J G, Xu T, *et al.*, 2017, Three Dimensional Electrospun PCL/PLA Blend Nanofibrous Scaffolds with Significantly Improved Stem Cells Osteogenic Differentiation and Cranial Bone Formation. *Biomaterials*, 115:115–27. https://doi.org/10.1016/j.biomaterials.2016.11.018
9. Ren K, Wang Y, Sun T, *et al.*, 2017, Electrospun PCL/Gelatin Composite Nanofiber Structures for Effective Guided Bone Regeneration Membranes. *Mater Sci Eng C Mater Biol Appl*, 78:324–32. https://doi.org/10.1016/j.msec.2017.04.084
10. Bean AC, Tuan RS, 2015, Fiber Diameter and Seeding Density Influence Chondrogenic Differentiation of Mesenchymal Stem Cells Seeded on Electrospun Poly (Epsilon-Caprolactone) Scaffolds. *Biomed Mater*, 10:015018. https://doi.org/10.1088/1748-6041/10/1/015018
11. Shanmugasundaram S, Chaudhry H, Arinzeh TL, 2011, Microscale Versus Nanoscale Scaffold Architecture for Mesenchymal Stem Cell Chondrogenesis. *Tissue Eng Part A*, 17:831–40. https://doi.org/10.1089/ten.TEA.2010.0409
12. Sisson K, Zhang C, Farach-Carson MC, *et al.*, 2010, Fiber Diameters Control Osteoblastic Cell Migration and Differentiation in Electrospun Gelatin. *J Biomed Mater Res A*, 94:1312–20. https://doi.org/10.1002/jbm.a.32756
13. He J, Zhang B, Li Z, *et al.*, 2020, High-Resolution Electrohydrodynamic Bioprinting: A New Biofabrication Strategy for Biomimetic Micro/Nanoscale Architectures and Living Tissue Constructs. *Biofabrication*, 12:042002. https://doi.org/10.1088/1758-5090/aba1fa
14. Abbasi N, Abdal-hay A, Hamlet S, *et al.*, 2019, Effects of Gradient and Offset Architectures on the Mechanical and Biological Properties of 3-D Melt Electrowritten (MEW) Scaffolds. *ACS Biomater Sci Eng*, 5:3448–61. https://doi.org/10.1021/acsbiomaterials.8b01456
15. Abbasi N, Ivanovski S, Gulati K, *et al.*, 2020, Role of Offset and Gradient Architectures of 3-D Melt Electrowritten Scaffold on Differentiation and Mineralization of Osteoblasts. *Biomater Res*, 24:2. https://doi.org/10.1186/s40824-019-0180-z
16. Mao M, He J, Li Z, *et al.*, 2020, Multi-Directional Cellular Alignment in 3D Guided by Electrohydrodynamically-Printed Microlattices. *Acta Biomater*, 101:141–51. https://doi.org/10.1016/j.actbio.2019.10.028
17. Brennan CM, Eichholz KF, Hoey DA, 2019, The Effect of Pore Size within Fibrous Scaffolds Fabricated Using Melt Electrowriting on Human Bone Marrow Stem Cell Osteogenesis. *Biomed Mater*, 14:065016. https://doi.org/10.1088/1748-605X/ab49f2
18. Eichholz KF, Hoey DA, 2018, Mediating Human Stem Cell Behaviour Via Defined Fibrous Architectures by Melt Electrospinning Writing. *Acta Biomater*, 75:140–51. https://doi.org/10.1016/j.actbio.2018.05.048
19. Xie C, Gao Q, Wang P, *et al.*, 2019, Structure-Induced Cell Growth by 3D Printing of Heterogeneous Scaffolds with Ultrafine Fibers. *Mater Des*, 181:108092. https://doi.org/10.1016/j.matdes.2019.108092
20. Zhang B, He J, Lei Q, *et al.*, 2019, Electrohydrodynamic Printing of Sub-Microscale Fibrous Architectures with Improved Cell Adhesion Capacity. *Virtual Phys Prototyp*, 15:62-74. https://doi.org/10.1080/17452759.2019.1662991
21. He J, Xu F, Dong R, *et al.*, 2017, Electrohydrodynamic 3D Printing of Microscale Poly (Epsilon-Caprolactone) Scaffolds with Multi-Walled Carbon Nanotubes. *Biofabrication*, 9:015007. https://doi.org/10.1088/1758-5090/aa53bc
22. Vijayavenkataraman S, Thaharah S, Zhang S, *et al.*, 2019, 3D-Printed PCL/rGO Conductive Scaffolds for Peripheral Nerve Injury Repair. *Artif Organs*, 43:515–23. https://doi.org/10.1111/aor.13360
23. Zhou Hand Lee J, 2011, Nanoscale Hydroxyapatite Particles for Bone Tissue Engineering. *Acta Biomater*, 7:2769–81. https://doi.org/10.1016/j.actbio.2011.03.019
24. Turnbull G, Clarke J, Picard F, *et al.*, 2018, 3D Bioactive Composite Scaffolds for Bone Tissue Engineering. *Bioact Mater*, 3:278–314. https://doi.org/10.1016/j.bioactmat.2017.10.001
25. Wu X, Miao L, Yao Y, *et al.*, 2014, Electrospun Fibrous Scaffolds Combined with Nanoscale Hydroxyapatite Induce Osteogenic Differentiation of Human Periodontal Ligament

Cells. *Int J Nanomed*, 9:4135–43.
https://doi.org/10.2147/IJN.S65272

26. Ribeiro Neto WA, Pereira IH, Ayres E, *et al.*, 2012, Influence of the Microstructure and Mechanical Strength of Nanofibers of Biodegradable Polymers with Hydroxyapatite in Stem Cells Growth. Electrospinning, Characterization and Cell Viability. *Polym Degrad Stab*, 97:2037–51.
https://doi.org/10.1016/j.polymdegradstab.2012.03.048
27. Li B, Chen Y, He J, *et al.*, 2020, Biomimetic Membranes of Methacrylated Gelatin/Nanohydroxyapatite/Poly(l-Lactic Acid) for Enhanced Bone Regeneration. *ACS Biomater Sci Eng*, 6:6737–47.
https://doi.org/10.1021/acsbiomaterials.0c00972
28. Lei Q, He J, Li D, 2019, Electrohydrodynamic 3D Printing of Layer-Specifically Oriented, Multiscale Conductive Scaffolds for Cardiac Tissue Engineering. *Nanoscale*, 11:15195–205.
https://doi.org/10.1039/c9nr04989d
29. Xia J, Yuan Y, Wu H, *et al.*, 2020, Decoupling the Effects of Nanopore Size and Surface Roughness on the Attachment, Spreading and Differentiation of Bone Marrow-Derived Stem Cells. *Biomaterials*, 248:120014.
https://doi.org/10.1016/j.biomaterials.2020.120014
30. Gao C, Peng S, Feng P, *et al.*, 2017, Bone Biomaterials and Interactions with Stem Cells. *Bone Res*, 5:17059.
https://doi.org/10.1038/boneres.2017.59
31. Tian F, Hosseinkhani H, Hosseinkhani M, *et al.*, 2008, Quantitative Analysis of Cell Adhesion on Aligned Micro- and Nanofibers. *J Biomed Mater Res A*, 84:291–9.
https://doi.org/10.1002/jbm.a.31304
32. Huang B, Aslan E, Jiang Z, *et al.*, 2020, Engineered Dual-Scale Poly (ε-Caprolactone) Scaffolds using 3D Printing and Rotational Electrospinning for Bone Tissue Regeneration. *Addit Manuf*, 36:101452.
https://doi.org/10.1016/j.addma.2020.101452
33. Oakes PW, Gardel ML, 2014, Stressing the Limits of Focal Adhesion Mechanosensitivity. *Curr Opin Cell Biol*, 30:68–73.
https://doi.org/10.1016/j.ceb.2014.06.003
34. Paluch EK, Aspalter IM, Sixt M, 2016, Focal Adhesion-Independent Cell Migration. *Annu Rev Cell Dev Biol*, 32:469–90.
https://doi.org/10.1146/annurev-cellbio-111315-125341
35. Revach OY, Grosheva I, Geiger B, 2020, Biomechanical Regulation of Focal Adhesion and Invadopodia Formation. *J Cell Sci*, 133:jcs244848.
https://doi.org/10.1242/jcs.244848
36. Sheets K, Wunsch S, Ng C, *et al.*, 2013, Shape-Dependent Cell Migration and Focal Adhesion Organization on Suspended and Aligned Nanofiber Scaffolds. *Acta Biomater*, 9:7169–77.
https://doi.org/10.1016/j.actbio.2013.03.042
37. Fu X, Liu G, Halim A, *et al.*, 2019, Mesenchymal Stem Cell Migration and Tissue Repair. *Cells*, 8:784.
https://doi.org/10.3390/cells8080784
38. Abedin E, Lari R, Shahri NM, *et al.*, 2018, Development of a Demineralized and Decellularized Human Epiphyseal Bone Scaffold for Tissue Engineering: A Histological Study. *Tissue Cell*, 55:46–52.
https://doi.org/10.1016/j.tice.2018.09.003
39. Blair HC, Larrouture QC, Li Y, *et al.*, 2017, Osteoblast Differentiation and Bone Matrix Formation *In Vivo* and *In Vitro*. *Tissue Eng Part B Rev*, 23:268–80.
https://doi.org/10.1089/ten.TEB.2016.0454
40. Oryan A, Kamali A, Moshiri A, *et al.*, 2017, Role of Mesenchymal Stem Cells in Bone Regenerative Medicine: What Is the Evidence? *Cells Tissues Organs*, 204:59–83.
https://doi.org/10.1159/000469704
41. Iaquinta MR, Mazzoni E, Bononi I, *et al.*, 2019, Adult Stem Cells for Bone Regeneration and Repair. *Front Cell Dev Biol*, 7:268.
https://doi.org/10.3389/fcell.2019.00268

Publisher's note